Science Advances
AAAS

advances.sciencemag.org/cgi/content/full/5/1/eaat5664/DC1

Supplementary Materials for

Microfluidic dielectrophoresis illuminates the relationship between microbial cell envelope polarizability and electrochemical activity

Qianru Wang, A.-Andrew D. Jones III, Jeffrey A. Gralnick, Liwei Lin, Cullen R. Buie*

*Corresponding author. Email: crb@mit.edu

Published 11 January 2019, *Sci. Adv.* **5**, eaat5664 (2019)
DOI: 10.1126/sciadv.aat5664

The PDF file includes:

Other Supplementary Material for this manuscript includes the following:

(available at advances.sciencemag.org/cgi/content/full/5/1/eaat5664/DC1)

Supporting figures

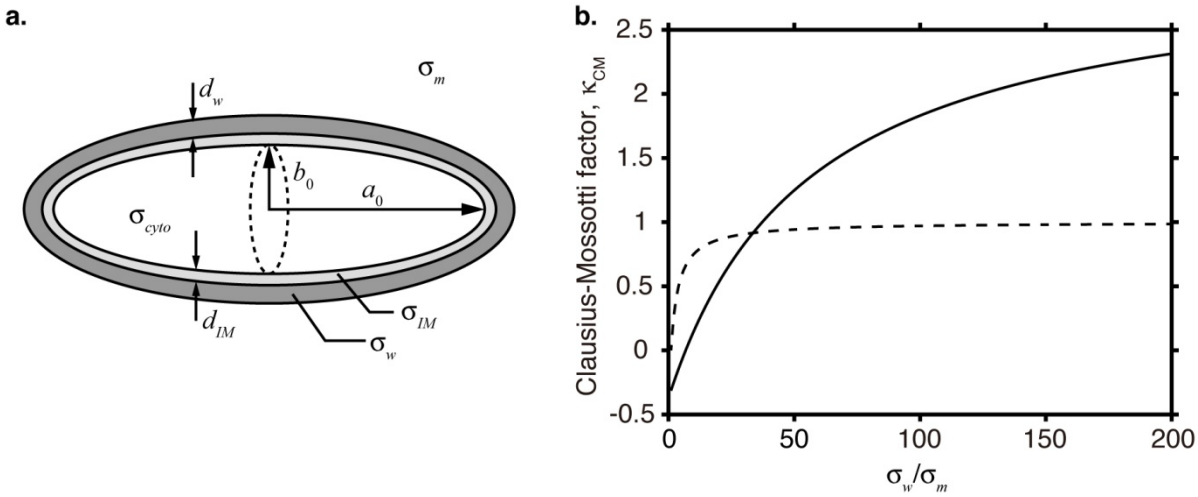

Fig. S1. The effect of cell shape on the Clausius-Mossotti factor. (**a**) A schematic of the two-shelled ellipsoidal model for bacteria (not drawn to scale). The bacterial cytoplasm is described as an ellipsoid with a major semi-axis a_0, minor semi-axis b_0, surrounded by an inner membrane layer of thickness d_{IM} and cell wall of thickness d_w. σ_{cyto}, σ_{IM}, σ_w and σ_m are conductivities of the cytoplasm, inner membrane, cell wall, and the surrounding medium, respectively. (**b**) Clausius-Mossotti factor (κ_{CM}) versus the ratio between conductivities of cell wall and surrounding medium ($\sigma_w/\ \sigma_m$) estimated by the two-shelled ellipsoidal model using Equation S8 in Section S1 (solid line) and the homogeneous spherical model (dashed line).

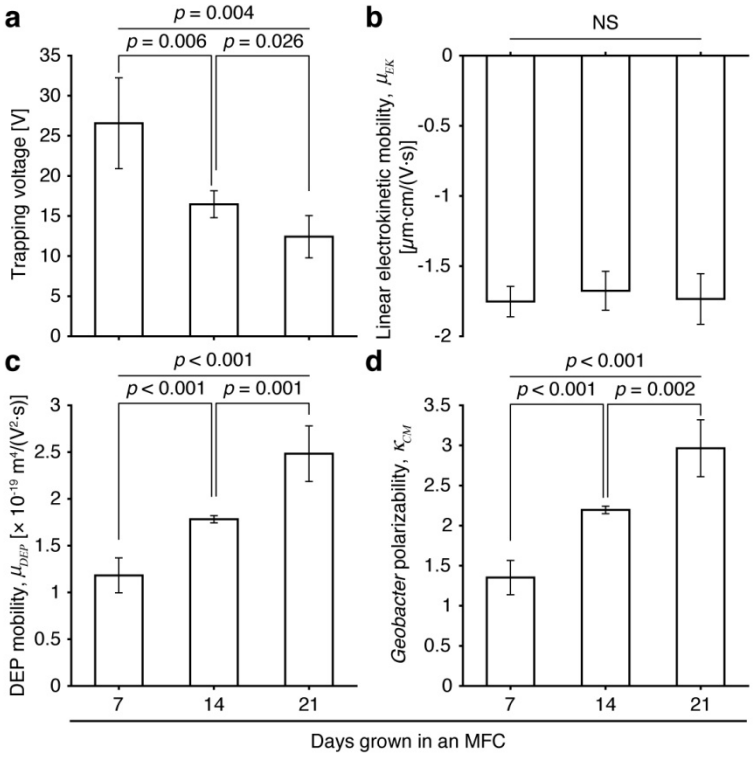

Fig. S2. MFC incubation time affects *G. sulfurreducens* polarizability. Trapping voltage (**a**), Linear electrokinetic mobility (**b**), DEP mobility (**c**), and cell polarizability (**d**) of *G. sulfurreducens* strain DL-1 harvested from an MFC anode with varying incubation time. Different from the growth condition corresponding to Fig. 2f, here DL-1 cells were maintained with Fe(III) oxide to be better adapted to reduce insoluble electron acceptors prior to the MFC incubation. Error bars indicate the standard deviation. Two-tailed *t*-test was performed with a sample size of $n = 4$.

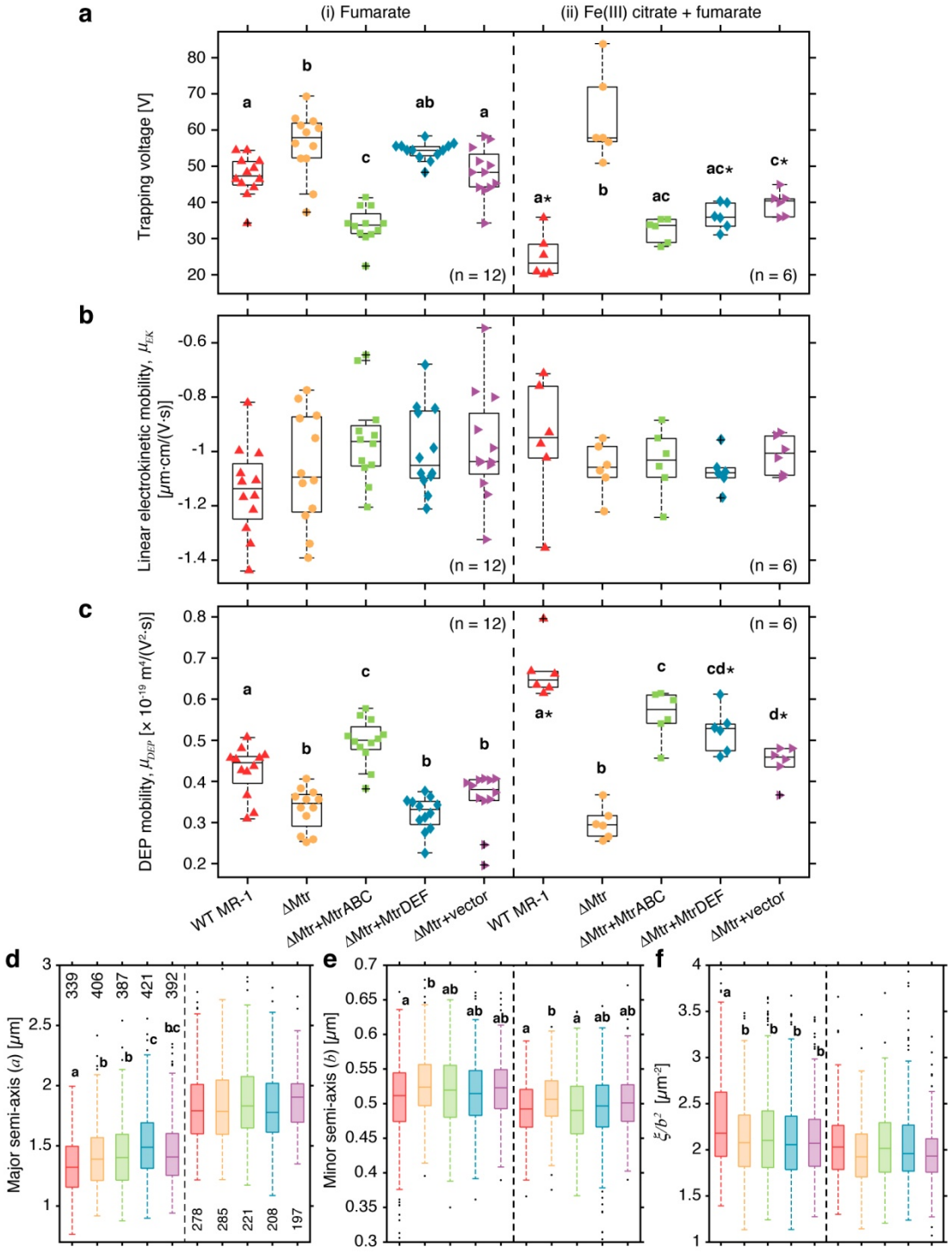

Fig. S3. *S. oneidensis* electrokinetics and cell morphology. (**a** to **c**) Trapping voltage (**a**), Linear electrokinetic mobility (**b**), and DEP mobility (**c**) of *S. oneidensis* wild type strain MR-1, strain deficient in expressing both MtrABC and MtrDEF EET conduits (ΔMtr), and ΔMtr complemented with indicated proteins (corresponding to Fig. 3c) grown with different electron accepters, namely, (i) 60 mM fumarate and (ii) 15 mM Fe(III) citrate supplemented with a small amount (10 mM) of fumarate. Bold letters above the box plots indicate results of a multiple

comparison test of group means using one-way ANOVA with a significance level of 0.05. Groups sharing a letter suggest no significant difference. Asterisk indicates significant difference ($p < 0.03$, two-tailed *t*-test) between the data of iron-reducing *S. oneidensis* (ii) and that of its fumarate-reducing counterpart (i). (**d** to **f**) Box-whisker plots of bacterial major semi-axis (**d**), minor semi-axis (**e**) and the ratio of Perrin friction factor to the square of short semi-axis ξ/b^2 (**f**) by ellipsoidal fit for the five investigated *S. oneidensis* strains. Numbers in panel (**d**) indicate the number of measured cells (*n*) for the cell morphology analysis. No significant difference was found between groups sharing a letter by a multiple comparison test of group means using Kruskal-Wallis with a significance level of 0.01.

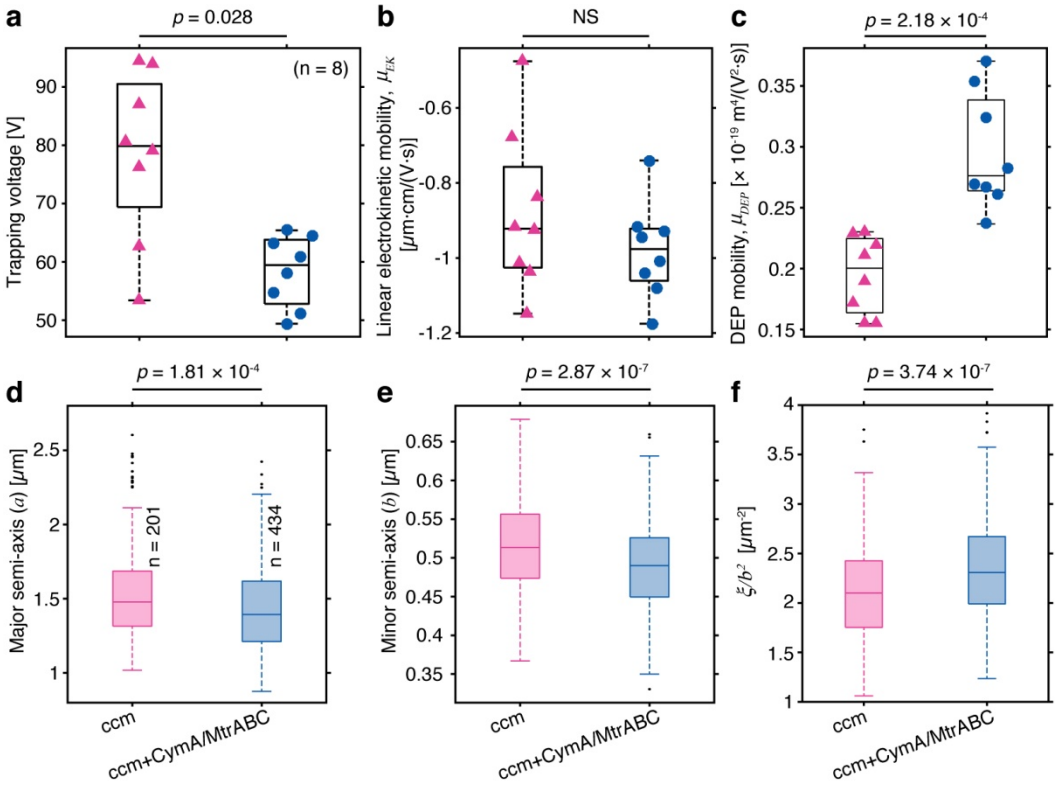

Fig. S4. Electrogenic *E. coli* electrokinetics and cell morphology. (**a** to **c**) Trapping voltage (**a**), Linear electrokinetic mobility (**b**), and DEP mobility (**c**) of the *E. coli* strain transformed with an empty cytochrome *c* maturation (*ccm*) plasmid (control) and the strain co-transformed with *S. oneidensis* MtrABC EET conduit grown with 15 mM Fe(III) citrate and 10 mM fumarate (corresponding to Fig. 4a, two-tailed *t*-test). (**d** to **f**) Box-whisker plots of bacterial major semi-axis (**d**), minor semi-axis (**e**) and the ratio of Perrin friction factor to the square of short semi-axis (**f**) by ellipsoidal fit for the investigated *E. coli* strains (two-tailed *t*-test). Numbers in panel (**d**) indicate the number of measured cells (*n*).

Supporting tables

Table S1. Summary of *G. sulfurreducens c*-type outer-membrane cytochromes in this study and their roles in EET.

C-type outer-membrane cytochromes	Location	Electron acceptor		Reference
		Fumarate/Fe(III) citrate/Fe(III) oxide	MFC anode [a)]	
OmcB	Tightly associated with the outer membrane, and partially exposed to the extracellular environment.	Crucial for optimal reduction of Fe(III) citrate and Fe(III) oxide. Facilitates electron transfer from the periplasm to the outer surface. Not required for fumarate-respiration (Fumarate reductase is either cytoplasmic or periplasmic, and so outer-membrane cytochromes are not involved). OmcB-deficient mutant never adapts to grow with Fe(III) oxide. Although it can gradually adapt to reduce soluble Fe(III) at a much lower growth rate, the loss of OmcB cannot be fully adapted.	Mediates heterogeneous EET across the biofilm/electrode interface. Expression level of *omcB* gene is significantly increased. Deletion of *omcB* has no impact on maximum current production.	8, 14-17
OmcE	Exposed on the outside of the cell.	Exclusively required for Fe(III) oxide reduction, but not for Fe(III) citrate. OmcE-deficient mutant gradually adapts to reduce Fe(III) oxide after 30 days of inoculation.	Not directly involved. The expression level of *omcE* is increased. Deletion of *omcE* has no impact on maximum current production.	9, 17
OmcS	Exposed on the outside of the cell, along the conductive pili.	Facilitates electron transfer from the pili to Fe(III) oxide. Not required for Fe(III) citrate reduction (the *omcS* gene is not expressed).	Plays a secondary role in homogeneous EET. The expression level is down-regulated. Deletion of *omcS* has no impact on maximum current production.	9, 16, 17
OmcT	Loosely bound to cell outer surface, with a negligible abundance compared to OmcS.	*OmcT* is immediately downstream of the *omcS* gene. Deleting either *omcS* or *omcT* negatively impacts expression of the other cytochrome gene. The presence of OmcT is not sufficient for Fe(III) oxide reduction.	Plays a secondary role in homogeneous EET. Expression of *omcT* is down-regulated.	9, 16
OmcZ	Exposed on the outside of the cell.	Not necessary for EET when cells are closely associated with the electron acceptor. Deletion of *omcZ* has no impact on cell growth with fumarate/Fe(III) citrate/Fe(III) oxide.	Indispensable for homogeneous EET through the thick biofilm bulk. Exhibits a much higher transcript abundance compared to the fumarate-grown cells. Loss of OmcZ severely inhibits current production and cannot be adapted. Simultaneous deletion of OmcB, OmcE, and OmcS can be adapted by increased abundance of OmcZ.	7, 17

a) Here describes *G. sulfurreducens* EET through relatively thick (ca. 50 μm) biofilms to MFC anodes, with high-density current production. Mechanisms for this long-range EET differ from that in the case where most of the cells are in direct contact with the electron acceptors.

Supporting video captions

Movie S1. 3DiDEP immobilization of *G. sulfurreducens*. (Left) A representative video showing the DL-1 cells were immobilized and gradually accumulated due to DEP near the microchannel constriction in response to the application of a 'linear sweep' DC potential difference (ramping rate, 1 V/s) across the microchannel (high potential applied to the right side). The red contours indicate the microchannel geometry, and the applied voltage and time are shown on the top-left and top-right corners, respectively. Scale bar, 100 μm. (Right) Fluorescence intensity (arbitrary unit, background subtracted) within the constricted region starts to increase with time when the 3DiDEP trapping is initiated. The threshold applied voltage at the onset of 3DiDEP immobilization is taken as the trapping voltage for the bacterial strain used. Video play speed is 6-folded increased.

Movie S2. Measurement of linear electrokinetic mobility using particle image velocimetry. (Left) A representative video showing the linear electrokinetic motion of DL-1 cells in a straight microfluidic channel driven by a DC potential difference started at t = 3 s from 3 V to 34 V with a ramping rate of 1 V/s. The green arrows indicate the velocity field measured by tracing the bacterial motion using PIV (arrows were plotted at every 3rd measurement point). The applied voltage and time are shown on the top-left corners. Scale bar, 50 μm. (Right) The average velocity measured using PIV was plotted against time (i.e. applied voltage), and was fitted linearly with the least squares method (dashed line). Red circles indicate the average of measured velocity fields, while blue bars extend to +/- 3x standard deviations. The best-fit slope was taken as the linear electrokinetic mobility for the bacterial strain used. Video play speed is 6-folded increased.

Section S1. Calculation of the Clausius-Mossotti factor for two-shelled ellipsoidal particles

Here we use a two-shelled prolate ellipsoid modal (*29*) to verify two hypothesises: 1) the Clausius-Mossotti factor for bacteria can be higher than one; and 2) the Clausius-Mossotti factor is dominated by cell surface (rather than internal) properties under DC electric fields.

Many authors estimate the Clausius-Mossotti factor being restricted from -0.5 to 1, but this is done assuming homogeneous spherical particles, which obviously disaccord with the facts of bacteria. A more reasonable simplification is to assume the bacterial cell as an ellipsoid of highly conductive cytoplasm enclosed by two concentric less conductive membranes with constant thickness (fig. S1a), and estimate the Clausius-Mossotti factor in three steps by implementing the Maxwell and Wagner theories at each interface of the neighboring layers. (*29*) Starting with the interface of the cytoplasm core and the inner membrane (IM) layer (fig. S1a), the effective dipole factor along the major axis of the ellipsoid can be expressed as

$$\kappa_1 = \frac{1}{3}\frac{\varepsilon^*_{cyto} - \varepsilon^*_{IM}}{\varepsilon^*_{IM} + A_1\left(\varepsilon^*_{cyto} - \varepsilon^*_{IM}\right)} \tag{S1}$$

where A_1 is the depolarization factor along the major axis of the ellipsoid given by

$$A_1 = \frac{1-e_1^2}{2e_1^3}\left[\log\left(\frac{1+e_1}{1-e_1}\right) - 2e_1\right] \tag{S2}$$

and the eccentricity is expressed by the major (a_0) and minor (b_0) semi-axes of the cytoplasm core (fig. S1a) as

$$e_1 = \sqrt{1-\left(\frac{b_0}{a_0}\right)^2}\,. \tag{S3}$$

Under DC electric fields, the complex permittivity of cytoplasm (ε^*_{cyto}) and the inner membrane

(ε^*_{IM}) in Equation S1 can be replaced by their corresponding conductivities (σ_{cyto} and σ_{IM}), respectively. The inner membrane is a phospholipid bilayer, and has a conductivity over three orders of magnitudes lower than the conductivity of cytoplasm for Gram-negative bacteria.(*29*, *46*) Thus, the inner membrane shell can be considered as electrically insulating, and Equation S1 is simplified as

$$\kappa_1 = \frac{1}{3A_1} \tag{S4}$$

Then the effective dipole factor in response to DC electric fields at the interface between the inner membrane and the cell wall (fig. S1a) is expressed as

$$\kappa_2 = \frac{1}{3}\frac{\left(\sigma_{IM}-\sigma_w\right)+3\kappa_1\rho_1\left[\sigma_{IM}+A_2\left(\sigma_w-\sigma_{IM}\right)\right]}{\sigma_w+A_2\left(\sigma_{IM}-\sigma_w\right)+3\kappa_1\rho_1A_2\left(1-A_2\right)\left(\sigma_{IM}-\sigma_w\right)} \tag{S5}$$

Again, the conductivity of the inner membrane (σ_{IM}) is much lower than the conductivity of the cell wall (σ_w),(*29*, *46*) and thus the dipole factor is simplified by

$$\kappa_2 = \frac{1}{3}\frac{3\kappa_1\rho_1A_2-1}{1-A_2-3\kappa_1\rho_1A_2\left(1-A_2\right)} = \frac{1}{3\left(A_2-1\right)} \tag{S6}$$

where the depolarization factor A_2 is again defined as in Equation S2 except that the eccentricity changes to

$$e_2 = \sqrt{1-\left(\frac{b_0+d_{IM}}{a_0+d_{IM}}\right)^2} \tag{S7}$$

with d_{IM} being the inner membrane thickness. ρ_1 is the volume ratio between the cytoplasm core and the ellipsoidal region enclosed by the outer surface of the inner membrane. Finally, the Clausius-Mossotti factor (i.e. the effective dipole factor along the ellipsoidal major axis) is expressed by the conductivity of the cell wall (σ_w) and the surrounding media (σ_m) as

$$\kappa_{CM} = \frac{1}{3}\frac{\left(\sigma_w - \sigma_m\right) + 3\kappa_2\rho_2\left[\sigma_w + A_3\left(\sigma_m - \sigma_w\right)\right]}{\sigma_m + A_3\left(\sigma_w - \sigma_m\right) + 3\kappa_2\rho_2 A_3\left(1 - A_3\right)\left(\sigma_w - \sigma_m\right)} \tag{S8}$$

where the depolarization factor A_3 is defined as in Equation S2 as before except that the eccentricity changes to

$$e_3 = \sqrt{1 - \left(\frac{b_0 + d_{IM} + d_w}{a_0 + d_{IM} + d_w}\right)^2} \tag{S9}$$

and the volume ratio is

$$\rho_2 = \frac{\left(a_0 + d_{IM}\right)\left(b_0 + d_{IM}\right)^2}{\left(a_0 + d_{IM} + d_w\right)\left(b_0 + d_{IM} + d_w\right)^2}. \tag{S10}$$

where d_w is the thickness of cell wall.

Cell wall for Gram-negative bacteria consists of the outer membrane, which is a lipid bilayer principally composed of lipopolysaccharide (LPS) in its outer leaflet and phospholipids in its inner leaflet (Fig. 1d and Fig. 3a). (*47*) The outer and inner membranes delimit the periplasmic space, an aqueous cellular compartment, which includes networks of peptidoglycan. (47) Unlike the inner membrane (a phospholipid bilayer), the abundance of charged groups (e.g. LPS), ion-exchangers (e.g. the outer-membrane cytochromes in *G. sulfurreducens*) and electrically conductive features (e.g. pilli) impart a much higher conductivity to the outer membrane compared to that of the inner membrane, which ensures that the Clausius-Mossotti factor measured by 3DiDEP using DC electric fields is dominated by cell surface properties. The ratio between conductivities of the cell surface and the surrounding medium (σ_w/σ_m) for *G. sulfurreducens* is high, which can result in a Clausius-Mossotti factor higher than 1. For instance, the conductivity of individual WT *G. sulfurreducens* pili is 51 ± 19 mS/cm, (*19*) which is more

than 500 times higher than that of the surrounding medium (ca. 0.1 mS/cm) used in this study. Using the cell dimensions averaged over all measured *G. sulfurreducens* strains in this study (a = 1.1 μm and b = 0.4 μm) and reported thicknesses of the inner membrane (ca. 5 nm) (*29*, *47*) and cell wall (ca. 35 nm, including a 25 nm thick periplasm and 10 nm thick outer membrane), (*48*) fig. S1b (solid line) shows the estimated Clausius-Mossotti factor for various ratios between the conductivities of the cell wall and the surrounding medium. Compared to the Clausius-Mossotti factor estimated by the spherical model (dashed line in fig. S1b) that is always lower than 1, the ellipsoidal model shows that the Clausius-Mossotti factor can be higher than 1. Additionally, the structure of bacterial outer membrane is far more complex than a homogeneous solid body. (*47*) The existence of soft polyelectrolyte layers can result in an even higher Clausius-Mossotti factor. (*39*)

Section S2. Microfluidic 3DiDEP device

The 3DiDEP device was fabricated by CNC micromachining a piece of poly (methyl methacrylate) (PMMA) sheet and bonding it with another blank PMMA chip using a solvent-assisted thermal binding process after cleaned both chips with acetone, methanol, isopropanol, and deionized (DI) water in sequence. Fluid reservoirs were then attached on top of the chips using a two-part epoxy (Fig. 1a). The channels are 1 cm in length, including a 50 μm long 3D constricted region with a cross-sectional area of 50 × 50 μm^2 in the center. The constriction bridges the two main channels where the cross-sectional area is 500 × 500 μm^2, yielding a constriction ratio of 100 (Fig. 1b). The high 3D constriction ratio enables high sensitivity for 3DiDEP characterization at low applied voltages. A more detailed description of the fabrication methods and channel geometry can be found elsewhere. (*27*, *28*) It is essential to maintain a consistent surface charge on the PMMA channel walls to generate constant electroosmotic flows. As a result, a conditioning process was performed before each 3DiDEP and linear electrokinetic mobility measurement. Each microchannel was flushed with 100 μM potassium hydroxide, DI water, and the DEP buffer solution sequentially at 500 μL/min for ten minutes. At the end of the process, bubbles were removed if presented in the channels, and excess buffer was removed from the reservoirs. Pressure difference across the microchannel was carefully eliminated before each experiment. The straight PMMA microchannels used for linear electrokinetic mobility measurements were 1 cm × 500 μm × 50 μm (length × width × depth), fabricated and primed using the same fabrication technique and conditioning process described above.